HHS Public Access

Author manuscript

Adv Mater. Author manuscript; available in PMC 2015 September 03.

Published in final edited form as:

Adv Mater. 2014 September 3; 26(33): 5815–5822. doi:10.1002/adma.201400941.

Bio-inspired Cryo-ink Preserves Red Blood Cell Phenotype and Function during Nanoliter Vitrification

Dr. Rami El Assal[#],
Bio-Acoustic-MEMS in Medicine (BAMM) Laboratory, Division for Biomedical Engineering, Division of Infectious Diseases, Renal Division, Department of Medicine, Brigham and Women's Hospital, Harvard Medical School, Harvard-Massachusetts Institute of Technology (MIT) Health Sciences and Technology, Cambridge, MA, 02139, USA

Dr. Sinan Guven[#],
Bio-Acoustic-MEMS in Medicine (BAMM) Laboratory, Division for Biomedical Engineering, Division of Infectious Diseases, Renal Division, Department of Medicine, Brigham and Women's Hospital, Harvard Medical School, Harvard-Massachusetts Institute of Technology (MIT) Health Sciences and Technology, Cambridge, MA, 02139, USA

Dr. Umut Atakan Gurkan,
Bio-Acoustic-MEMS in Medicine (BAMM) Laboratory, Division for Biomedical Engineering, Division of Infectious Diseases, Renal Division, Department of Medicine, Brigham and Women's Hospital, Harvard Medical School, Harvard-Massachusetts Institute of Technology (MIT) Health Sciences and Technology, Cambridge, MA, 02139, USA, Case Western Reserve University, Biomanufacturing and Microfabrication Laboratory, Mechanical and Aerospace Engineering Department, Department of Orthopedics, Advanced Platform Technology Center, Louis Stokes Cleveland Veterans Affairs Medical Center, Cleveland, OH, 44106 USA

Dr. Irep Gozen,
Bio-Acoustic-MEMS in Medicine (BAMM) Laboratory, Division for Biomedical Engineering, Division of Infectious Diseases, Renal Division, Department of Medicine, Brigham and Women's Hospital, Harvard Medical School, Harvard-Massachusetts Institute of Technology (MIT) Health Sciences and Technology, Cambridge, MA, 02139, USA

Dr. Hadi Shafiee,

---

[*]utkan@stanford.edu, udemirci@rics.bwh.harvard.edu.
[#]Current address: Bio-Acoustic-MEMS in Medicine (BAMM) Laboratory, Canary Center at Stanford for Cancer Early Detection, Department of Radiology, Stanford University School of Medicine, Palo Alto, CA, 94304, USA

Conflict-of-interest statement

Dr. Utkan Demirci is a founder of, and has an equity interest in, DxNow, a company that is developing microfluidic and imaging technologies for point-of-care diagnostic solutions. Dr. Utkan Demirci's interests were viewed and managed by the Brigham and Women's Hospital and Partners HealthCare in accordance with their conflict of interest policies. Dr. Utkan Demirci is a scientific advisory board member of Akron Biotechnology. Dr. Claudia Zylberberg is the Chief Executive Officer of Akron Biotechnology. Akron Biotechnology provided the ectoin solution.

Author contributions

R.E and U.D. developed the idea; R.E, S.G, U.A.G, N.L, R.K, Q.W, and U.D. designed the experimental approach; R.E, S.G, U.A.G, H.S, S.D, N.A, G.T, J.E, J.K, Q.W, W.F, G.T, and Q.W. performed the experiments; R.E, S.G, U.A.G, I.G., G.T, B.I, R.K, C.Z, N.L, Q.W, and U.D. analyzed the data; R.E, S.G, U.A.G, I.G, S.D, N.A, W.F, Q.W, I.G, and U.D. wrote the manuscript.

Supporting Information

Supporting Information is available from the Wiley Online Library or from the author.

Bio-Acoustic-MEMS in Medicine (BAMM) Laboratory, Division for Biomedical Engineering, Division of Infectious Diseases, Renal Division, Department of Medicine, Brigham and Women's Hospital, Harvard Medical School, Harvard-Massachusetts Institute of Technology (MIT) Health Sciences and Technology, Cambridge, MA, 02139, USA

Sedef Dalbeyber,
Bio-Acoustic-MEMS in Medicine (BAMM) Laboratory, Division for Biomedical Engineering, Division of Infectious Diseases, Renal Division, Department of Medicine, Brigham and Women's Hospital, Harvard Medical School, Harvard-Massachusetts Institute of Technology (MIT) Health Sciences and Technology, Cambridge, MA, 02139, USA

Noor Abdalla,
Bio-Acoustic-MEMS in Medicine (BAMM) Laboratory, Division for Biomedical Engineering, Division of Infectious Diseases, Renal Division, Department of Medicine, Brigham and Women's Hospital, Harvard Medical School, Harvard-Massachusetts Institute of Technology (MIT) Health Sciences and Technology, Cambridge, MA, 02139, USA

Gawain Thomas,
Department of Physics, Worcester Polytechnic Institute, Worcester, MA, 01609 USA

Wendy Fuld,
Department of Pathology, Brigham and Women's Hospital, Harvard Medical School, Boston, MA, 02115 USA

Dr. Ben M.W. Illigens,
Department of Neurology, Beth Israel Deaconess Medical Center, Harvard Medical School, Boston, MA, 02215 USA

Jessica Estanislau,
Division of Infectious Disease and Allergy-Inflammation, Department of Medicine, Beth Israel Deaconess Medical Center, Harvard Medical School, Boston, MA, 02115 USA

Joseph Khoory,
Division of Infectious Disease and Allergy-Inflammation, Department of Medicine, Beth Israel Deaconess Medical Center, Harvard Medical School, Boston, MA, 02115 USA

Dr. Richard Kaufman,
Brigham and Women's Hospital Blood Bank, Division of Adult Transfusion Medicine, Department of Pathology, Brigham and Women's Hospital, Harvard Medical School, Boston, MA, 02115 USA

Dr. Claudia Zylberberg,
Akron Biotechnology, LLC, Boca Raton, FL, 33487 USA

Dr. Neal Lindeman,
Department of Pathology, Brigham and Women's Hospital, Harvard Medical School, Boston, MA, 02115 USA

Dr. Qi Wen,
Department of Physics, Worcester Polytechnic Institute, Worcester, MA, 01609 USA

Dr. Ionita Ghiran, and

Division of Infectious Disease and Allergy-Inflammation, Department of Medicine, Beth Israel Deaconess Medical Center, Harvard Medical School, Boston, MA, 02115 USA

Dr. Utkan Demirci[*,#]
Bio-Acoustic-MEMS in Medicine (BAMM) Laboratory, Division for Biomedical Engineering, Division of Infectious Diseases, Renal Division, Department of Medicine, Brigham and Women's Hospital, Harvard Medical School, Harvard-Massachusetts Institute of Technology (MIT) Health Sciences and Technology, Cambridge, MA, 02139, USA

Abstract

Current red blood cell cryopreservation methods utilize bulk volumes, causing cryo-injury of cells, which results in irreversible disruption of cell morphology, mechanics, and function. An innovative approach to preserve human red blood cell morphology, mechanics, and function following vitrification in nanoliter volumes is developed using a novel cryo-ink integrated with a bio-printing approach.

Keywords

Bio-inspired material; Cryoprotective agent; Nanoliter vitrification; Bioprinting; Red blood cell cryopreservation

The unique morphology and mechanics of red blood cells (RBCs) are critical in influencing their function [1] . Recent studies have revealed detrimental alterations in RBC morphological, mechanical, and functional properties (collectively termed as "storage injury") during RBC hypothermic liquid preservation [2]. Such adverse storage changes correlate with increased mortality and morbidity rates in medically compromised patients when RBCs are stored for more than 14 days [3].

Cryopreservation has emerged as an alternative approach that extends the preservation period for years by overcoming the adverse changes that occur in liquid preservation. Although RBC cryopreservation is clinically employed, adverse morphological [4], mechanical [5], and functional [6] changes still present challenges. Current RBC cryopreservation techniques utilize glycerol in slow freezing [7] and rapid freezing techniques [8]. Several causative factors have been shown to be involved in cryo-injury, however, cryoprotective agent (CPA) use, and cooling and rewarming approaches are detrimental [9]. In contrast, vitrification, by which cells are transformed into a glassy-state, has emerged as an alternative to the presently applied means of cryopreservation. However, conventional vitrification requires high concentrations of CPAs to achieve successful vitrification. CPA acts as antifreeze to the cytosol and as a stabilizer for the plasma membrane; but it is toxic to cells when used in high concentrations [9,10]. Although vitrification has been used and shown advantages over traditional cryopreservation techniques, it has not been incorporated into transfusion medicine mainly due to inability to achieve vitrification with bulk volumes and throughput challenges. Therefore, innovative technologies for vitrification could improve RBC preservation success, which is urgently needed to advance the clinical practice of transfusion medicine and expand RBC

preservation options for patients. Moreover, the use of bio-inspired materials in this context can offer additional benefits [11].

Recent advances in manipulating cells and droplets have been made particularly at the interface between bioengineering, biomaterials and medicine [12]. In one important instance, a new high technology-enabled capability of printing viable and functional cells has been reported [13]. In the present study, we report the preservation of human RBC morphology, mechanics, and function following vitrification using a novel cryo-ink integrated with cryo-printer, a droplet generation tool that can transform a bulk volume of human blood into nanoliter droplets on a cryo-paper. The results reveal that the recovered RBCs after ectoine-assisted vitrification, maintained their characteristic features such as morphology, submembranous spectrin-actin network as well as mechanical properties. In addition, the essential functions of recovered RBCs such as phosphorylation of band-3 protein, expression of complement receptor 1, and maintenance of intracellular nitric oxide and the reactive oxygen species are effectively preserved.

To transform a bulk sample of RBCs into nanoliter volume droplets in a bio-inspired cryo-ink, we developed a cryo-printing methodology (Figure 1). In this method, the cryo-ink acts as a cryoprotective agent to help the cells overcome the shock during the cooling and rewarming processes of cryopreservation. The cryo-printer contains an ejector in which the RBC-CPA mixture and the nitrogen gas are simultaneously expelled leading to the formation of nanoliter size droplets at the ejector outlet (Figure 1a). The cryo-printer in our experiments produces considerably small volumes of droplets (0.14±0.096 nL, Figure S1), with the aim to minimize the adverse effects on RBCs by eliminating the requirements of high CPA concentrations to achieve vitrification. Vitrification by using nanoliter droplets requires low concentrations of CPA (4.5%) while conventional methods, which utilize bulk volumes (450–500ml), require high concentrations of CPAs (20–40%). Such high concentrations of CPAs loaded into bulk samples for conventional methods have been reported to cause adverse effects on RBCs [14]. In addition, small volumes of droplets provide ultra-high cooling and rewarming rates that enable preserving cells without ice crystal formation.

Prior to cooling, blood samples were loaded with a cryo-protective ink at 1:1 dilution. A possible osmotic shock emerging from the exposure to the cryo-ink that would lead to RBC loss, was evaluated via hemolysis and revealed to be insignificant (Figure S2). This cryo-ink contains ectoine (9% v/v), trehalose (25 μg/mL), and polyethylene glycol (PEG, 1% v/v) (Figure 1b). The optimal concentration of ectoine in the cryo-ink was determined as a result of a set of hemolysis analysis (Figure S3). Ectoine is a naturally occurring solute present in the extremophilic bacteria which are capable of adapting to extreme thermal and osmotic stress conditions [15]. This is associated with the preferential exclusion of ectoine at the interface of a lipid monolayer of the cell membrane. The exclusion leads to the expansion of the membrane promoting the water molecules to penetrate [16,17]. The increased number of water molecules in the vicinity of the lipids improve the membrane fluidity which is crucial to withstand osmotic shock and to assist in the cell repair mechanisms [16]. Ectoine-containing CPA solutions have previously been employed for mesenchymal stem cell preservation with conventional slow freezing protocols [11]. The cryo-ink solution used in

this study contains in addition to ectoine, trehalose and PEG which have complementary enhancing effects [18,19]. For example, PEG suppress the freezing point of the solution [19]. We utilized vitrification (below −150 °C) as a cooling method instead of conventional freezing (−80°C or above) to minimize cryo-injury. Vitrification occurs when the CPA-loaded RBCs are super-cooled down to the glass transition temperature and adopt a glass-like amorphous morphology [10]. This is different than conventional freezing where the cell injury, caused by the formation of ice crystals, is of concern [10,20]. The printing of the nanoliter droplets on a cryo-paper (polyethylene collection film) and subsequent submersion into liquid nitrogen (−196 °C) results in immediate vitrification of the RBCs (Figure 1c). One of the major challenges in conventional vitrification is ice crystallization, which occurs during rapid rewarming [10]. The ice crystallization occurs as a result of the latent heat of fusion, causing hemolysis of the cells [10]. To avoid such crystallization, the vitrified blood sample was ultra-rapidly rewarmed by immersing the printed nanoliter droplets on the cryo-paper in warm media (≥37 °C) (Figure 1b). Furthermore, utilizing bio-inspired CPAs; such as ectoine and trehalose, in low concentrations eliminates extensive washing steps that are required for other protocols such as glycerol-based techniques. The washing step is minimal in this method and was achieved by re-suspending the RBCs in PBS.

The extent of cryo-injury on RBCs is reflected by their altered morphology. Healthy RBCs have a unique biconcave-discoid morphology (Figure 2a, i, m and Figure, S5, S6, and S7). The biconcave shape increases oxygen-delivering capacity of RBCs provided by the high surface area in close proximity to the vessel walls [21]. Additionally, RBCs owe their extreme flexibility to their biconcave shape [22], which allows them to travel through microvasculature. If RBCs are challenged by mild environmental fluxes such as slight osmotic changes [23], reversible morphological alterations may occur. One example is the transformation to echinocytes (Figure S4), where the plasma membrane exhibits small projections [24]. Irreversible shape changes of RBCs are indicated by the formation of spherocytes, the completely round forms of RBCs [25]. To investigate the changes in morphology of recovered RBCs subsequent to ectoine-based vitrification (EV), a series of scanning electron micrographs (SEM) were obtained (Figure 2a–d and Figure. S5a–r). The cells visualized by SEM were categorized under 3 different groups: cells exhibit (i) no change (biconcave discocyte), (ii) reversible change (e.g., echinocyte and stomatocyte), and (iii) irreversible (spherocyte) change [26]. For each group, the number of recovered cells was considered to be the total count of the biconcave RBCs and the RBCs that exhibit reversible changes. Approximately, 94% of the RBCs in the fresh blood sample have the characteristic RBC morphology (Figure 2e). Likewise, approximately 88% of RBCs during the EV maintained their original form (Figure 2f). We compared our results to alternative cryopreservation methods including low glycerol vitrification (LGV) and low glycerol slow freezing (LGSF). The RBCs recovered after LGV and LGSF go through significant irreversible shape changes (mainly spherocytes): 83% and 88% of the entire population of cells, respectively (Figure 2g, h). This is in agreement with the previous observations of the transformation of biconcave human RBCs [4] and mesenchymal stem cells [11] to spherocytes upon glycerol-based cryopreservation. Figure 2i–l include high magnification SEMs of the recovered RBCs. SEMs of RBCs with various magnifications during each step in cryopreservation protocols are also shown in Figure S5. To evaluate the topographical

maps of recovered RBCs, we have performed atomic force microscopy (AFM) (Figure 2m–p). The results are in agreement with the SEM observations and confirm the biconcave shape of cells in the control group and of the recovered cells after EV. The maps show cells that experienced LGV and LGSF became spherocytes. Spherocytes are undesired forms of RBCs and such irreversible shape changes of RBCs are related to decreased function and diseases: studies investigating the impact of irreversibly altered RBC morphology after transfusion of stored blood have reported a reduced capacity of RBCs to oxygenate the tissues [27], increasing the risk for peripheral ischemia and deep venous thrombosis [28]. Spectrin and actin proteins construct the major backbone of the RBC skeleton which collapses when these proteins are damaged [22]. To investigate the effect of EV on the RBC cytoskeleton, we performed immunocytochemistry to evaluate the distribution of spectrin (α- and β-chains) and actin filaments of recovered cells (Figure 2q–t). The pattern distribution across the recovered RBCs after EV was comparable to the control RBCs (Figure 2q, r). The RBCs recovered after LGV and LGSF showed different protein distribution patterns where the central spectrin-actin region was distorted (Figure 2s) or disintegrated (Figure 2t and Figure S6).

To test the mechanical properties of recovered RBCs, we evaluated the membrane stiffness, cell deformability, and membrane flickering. Cell stiffness was evaluated by measuring the elastic moduli of the cells using AFM. The stiffer the cell, the higher its elastic modulus [29]. Recovered RBCs after EV displayed comparable stiffness (461±38 Pa) to control RBCs (358±38 Pa) (Figure 3a). The recovered cells were incubated in autologous plasma for 3 hours to evaluate the membrane stiffness *ex vivo*. On the other hand, RBCs recovered after LGSF displayed greater ($p<0.05$) stiffness (879±47 Pa, Figure 3a) compared to the control. Another characteristic of RBCs is their significant deformability which enables them to pass through capillary veins, exchange oxygen and carbon dioxide with cells in tissues [30]. We have measured the deformability by forcing the recovered RBCs to pass through 4.5μm wide and 2μm high microchannels (Figure 3b) and by evaluating the duration of their travel along the channels (Figure 3c). This evaluation is based on the findings from previous reports [31] which indicate a relatively more flexible cell would be able to pass through the channel in a shorter time, compared with a less-deformable cell. The RBCs recovered from EV passed through the microfluidic channels by 1.3 seconds faster on average compared with control RBCs (Figure 3c). The difference is statistically significant ($p<0.05$) and indicates higher deformability of the recovered cells after EV. The measurements were performed on the fresh blood at room temperature (20–24 C°). The corresponding measurements on recovered RBCs from EV have been performed also at room temperature but after the cells experienced significant temperature changes during cooling and rewarming (−198 C° to 37 C°). The increase in the deformability of RBCs measured in a similar microfluidic system was linked to temperature changes [32]. An increase in RBC deformability was previously investigated but was not linked to negative effects [5,33] whereas a decrease in deformability was associated with blood related diseases [30,34] and low quality of stored blood [2]. The analysis on the deformability of the RBCs could not be performed for the LGV and LGSF due to blockage of microchannels by the RBCs in these two groups. Earlier reports have associated the reduced deformability in stored RBCs with irreversible shape changes, such as those observed for spherocytes [35].

The membrane flickering of recovered cells, also known as fluctuations or oscillations, was evaluated as a functional response of RBCs [36]. The flickering was quantified by recording changes in light scattering at the surface of a RBC using time-lapse, positive-low phase contrast microscopy over a period of 30 seconds at frequency of 33 frames/second (Figure 3d–l). The intensity of scattered light was used to calculate the coefficient of variance at each point. These fluctuations show that the recovered RBCs after EV maintained their flickering amplitude at levels comparable with fresh RBCs (Figure 3d). However, the amplitude of membrane flickering in the recovered cells after LGV and LGSF differs significantly ($p<0.05$) from both control and recovered RBCs after EV (Figure 3d). Loss of flickering amplitude has been observed in RBCs during multiple diseases such as systemic lupus erythematosus and malaria infection [30,37]. The pseudo-color images in Figure 3e–h represent a map of the coefficient of variance on the RBCs measured as a sum of each pixel covering the cell surface during 30 seconds. Figure 3i–l shows the amplitude of intensity of a representative pixel corresponding to the pseudo-color images in Figure 3e–h.

To evaluate the functional properties of EV recovered RBCs, we measured band-3 phosphorylation (Figure 4a), CD35 expression (Figure 4b), intracellular nitric oxide (NO) (Figure 4c), and intracellular reactive oxygen species (ROS) (Figure 4d). The measurements were performed by flow cytometry after incubation in 25% serum from a known universal donor. Band-3 is an integral protein that regulates RBC membrane organization and function [38]. Alteration of band-3 phosphorylation levels has been associated with increased rigidity of RBCs, therefore, decreasing their perfusion to host organs and their lifespan in the circulation [39]. Although there was a slight decrease of band-3 phosphorylation level in recovered RBCs after EV (geometric mean: 25) compared to control RBCs (geometric mean: 29.7), the decrease was not significant (Figure 4a). CD35 (also known as complement receptor 1, CR1), is an unique human RBC regulatory protein [40], critical in the immune-clearance process and thus for the maintenance of a non-inflammatory intravascular environment [41]. Injury associated with RBC storage changes the tendency of CD35 to cluster on the cell membrane, which reduces the ability of the cell to capture and transport the inflammatory particles, thereby maintaining the non-inflammatory status of the circulatory system [41]. The recovered RBCs after EV showed a comparable CD35 expression level to the control RBCs that were collected from the same donor with a geometric mean of 7.5 and 8.0, respectively (Figure 4b).

The intracellular NO and ROS levels as regulators for blood flow and RBC homeostasis, were also evaluated [42]. NO is a crucial short-lived signaling molecule regulating the local vasodilation [43]. Loss of NO has been observed after a prolonged storage of RBCs and it has been linked to biochemical (e.g., depletion of adenosine triphosphate and 2,3 diphosphoglycerate) or hemolysis-related changes including morphology and deformability changes [44]. Formation of ROS during the preservation process has been also shown to accelerate RBC storage injury, and significantly reduce post-transfusion RBC viability [45]. ROS are highly reactive molecules that target a wide range of cell components including lipids, nucleic acids and proteins (i.e., spectrin in RBCs), which undergo irreversible ROS-mediated changes resulting in significant decreases in RBC deformability [46]. Our results demonstrated that the cells recovered after EV maintained the intracellular NO (geometric mean: 9.6) and ROS levels (geometric mean: 6.7) compared to control RBCs (geometric

mean: 8.8 and 7.2, respectively) (Figure 4b–d). In addition, flow cytometer results clearly reveal the preservation of recovered RBC morphology after EV, fully supporting our SEM and AFM results shown in Figure. 1 (Figure S7).

In this study, we report the preservation of human red blood cell (RBC) morphology, mechanics, and function following vitrification in nanoliter volumes using an innovative cryo-ink integrated with a bio-printing approach. The use of nano-liter droplet vitrification for the purpose of cryopreservation of RBCs has not been well studied or applied [10], although it could potentially provide a powerful means to cryopreserve RBCs for blood banking. One challenge is the transformation of the concept into a high throughput system where large volumes of blood are rapidly vitrified. We have previously demonstrated the scalability of droplet system by developing arrays consisting of multiple ejectors for droplet generation, which potentially enables automation and high throughput processing [47]. We envision that a series of such arrays would provide rapid printing of droplets for the bulk volumes of blood samples before vitrification. Furthermore, the presented method has the potential to minimizes cell contamination by using sterilize liquid nitrogen (LN_2). It has been shown that LN_2 can be sterilized by utilizing ultra-violet radiation [48], or sterile PTFE cartridge filters [49], minimizing such contamination risks [50]. Therefore, the presented method has the potential for minimizing such contamination risks and allowing the sterilization of potential automated high throughput applications by bringing multiple ejectors together. Additionally, we observed a mild increase in the hemolysis when using the polyethylene collection film (Figure S8). We think the hemolysis at this collection step may be eliminated with the use of materials that would enable less mechanical stress upon collection, for example a soft and biocompatible fibrin film. The RBCs cryo-printing step was also evaluated and compared with manually pipetting of CPA loaded RBCs (control). None of the printed groups (EV and LGV) show significant increase in hemolysis above the acceptable level, thereby validating the cryoprinting-based system (Figure S8).

Here, we demonstrated the cryo-printing of the ectoine-loaded RBCs encapsulated in nanoliter droplets. The printed RBCs on cryo-paper were vitrified in extremely low temperatures and after rewarming the maintenance of RBC morphology, mechanics and function were evaluated. The ectoine assisted cryo-printing has potential to improve efficiency of blood banking and further create new approaches to biopreserve various cell types including stem cells and gametes.

Supplementary Material

Refer to Web version on PubMed Central for supplementary material.

Acknowledgments

This work was performed at the Bio-Acoustic MEMS in Medicine (BAMM) Labs at the HST-BWH, Harvard Medical School. The authors would like to acknowledge their appreciation to the late-Dr. Aida Nureddin for her significant contributions to this project. She was instrumental in the design, execution and interpretation of this data. Dr. Nureddin’s intellect and pleasant demeanor will be sorely missed. We would like also to thank April Holland, Maria Lebruto, Mark Melhon, Burcu Erkmen, Vasily Giannakeas, Josh Samot, Waseem Asghar, Zhang Xu, Fatih Inci, Andrea Pena, and Sandra Boehler for technical support and discussion through out the research project. We would like to thank Quang Le, Daniel Martinenz and Hassan Sakhta for contributing in this study as high school students under the Student Success Job Program at Brigham and Women's Hospital, Harvard Medical

School and under Dr. Demirci's NSF Career Award # 1150733. We would also like to thank Mudit Tandon from Belmont Hill School for his contributing to this study. Following this study Quang Lee, Daniel Martinenz, and Mudit Tandon joined University of Massachusetts, Harvard University and Tuft University for their college education, respectively. This work was partially supported by NIH R21-HL095960, NIH R01-EB015776, NIH R01-HL096795 and Swedish Research Council-Vetenskapsrådet.

References

1. Discher D, Mohandas N, Evans E. Science. 1994; 266:1032. [PubMed: 7973655] Mohandas N, Chasis J. Red blood cell deformability, membrane material properties and shape: regulation by transmembrane, skeletal and cytosolic proteins and lipids. presented at Seminars in hematology. 1993
2. Bennett-Guerrero E, Veldman TH, Doctor A, Telen MJ, Ortel TL, Reid TS, Mulherin MA, Zhu H, Buck RD, Califf RM, McMahon TJ. Proc Nat Acad Sci USA. 2007; 104:17063. [PubMed: 17940021]
3. Koch CG, Li L, Sessler DI, Figueroa P, Hoeltge GA, Mihaljevic T, Blackstone EH. New Engl J Med. 2008; 358:1229. [PubMed: 18354101]
4. Pallotta V, D'Amici GM, D'Alessandro A, Rossetti R, Zolla L. Blood Cells, Molecules, and Diseases. 2012; 48:226.
5. Henkelman S, Lagerberg JW, Graaff R, Rakhorst G, Van Oeveren W. Transfusion. 2010; 50:2393. [PubMed: 20561300]
6. Holovati JL, Wong KA, Webster JM, Acker JP. Transfusion. 2008; 48:1658. [PubMed: 18482179]
7. Meryman HT, Hornblower M. Transfusion. 1972; 12:145. [PubMed: 5026166]
8. Rowe AW, Eyster E, Kellner A. Cryobiology. 1968; 5:119. [PubMed: 5717951]
9. Scott KL, Lecak J, Acker JP. Transfusion Medicine Reviews. 2005; 19:127. [PubMed: 15852241]
10. Meryman HT. Transfusion. 2007; 47:935. [PubMed: 17465961]
11. Grein TA, Freimark D, Weber C, Hudel K, Wallrapp C, Czermak P. The International journal of artificial organs. 2010; 33:370. [PubMed: 20669142]
12. Gurkan UA, El Assal R, Yildiz SE, Sung Y, Trachtenberg AJ, Kuo WP, Demirci U. Molecular pharmaceutics. 2014Ceyhan E, Xu F, Gurkan UA, Emre AE, Turali ES, El Assal R, Acikgenc A, Wu C-aM, Demirci U. Lab Chip. 2012; 12:4884. [PubMed: 23034772] Gurkan, U.; Sung, Y.; El Assal, R.; Xu, F.; Trachtenberg, A.; Kuo, W.; Demirci, U. Bioprinting anisotropic stem cell microenvironment. presented at Journal of Tissue Engineering and Regenerative Medicine; 2012.
13. Durmus NG, Tasoglu S, Demirci U. Nat Mat. 2013; 12:478.
14. Mantzavinos D, Bailey A, Rampling M. Biorheology. 1997; 34:73. [PubMed: 9176591]
15. Lippert K, Galinski EA. Applied microbiology and biotechnology. 1992; 37:61.
16. Harishchandra RK, Wulff S, Lentzen G, Neuhaus T, Galla HJ. Biophysical chemistry. 2010; 150:37. [PubMed: 20206435]
17. Pastor JM, Salvador M, Argandoña M, Bernal V, Reina-Bueno M, Csonka LN, Iborra JL, Vargas C, Nieto JJ, Cánovas M. Biotechnology advances. 2010; 28:782. [PubMed: 20600783]
18. Bhandal IS, Hauptmann RM, Widholm JM. Plant physiology. 1985; 78:430. [PubMed: 16664260]
19. Ohboshi S, Fujihara N, Yoshida T, Tomogane H. Animal reproduction science. 1997; 48:27. [PubMed: 9412730]
20. Pegg, DE. Cryopreservation and Freeze-Drying Protocols. Springer; 2007. p. 39Karlsson JO, Toner M. Biomaterials. 1996; 17:243. [PubMed: 8745321]
21. Guest MM, Bond TP, Cooper RG, Derrick JR. Science. 1963; 142:1319. [PubMed: 14074848]
22. Mohandas N, Gallagher PG. Blood. 2008; 112:3939. [PubMed: 18988878]
23. Mrowietz C, Hiebl B, Franke R, Park JW, Jung F. Clinical hemorheology and microcirculation. 2008; 39:281. [PubMed: 18503136]
24. Stasiuk M, Kijanka G, Kozubek A. Postepy biochemii. 2009; 55:425. [PubMed: 20201356]
25. Cluitmans JC, Hardeman MR, Dinkla S, Brock R, Bosman GJ. Blood transfusion = Trasfusione del sangue. 2012; 10(Suppl 2):s12. [PubMed: 22890263]

26. Bessis M. Nouvelle revue francaise d'hematologie. 1972; 12:721.Laczko J, Feo C, Phillips W. Transfusion. 1979; 19:379. [PubMed: 473341]
27. Tinmouth A, Fergusson D, Yee IC, Hébert PC. Transfusion. 2006; 46:2014. [PubMed: 17076859] Bosman G, Werre J, Willekens F, Novotný V. Transfusion Medicine. 2008; 18:335. [PubMed: 19140816]
28. Alt E, Banyai S, Banyai M, Koppensteiner R. Thrombosis research. 2002; 107:101. [PubMed: 12431474] Yedgar S, Koshkaryev A, Barshtein G. Pathophysiology of haemostasis and thrombosis. 2003; 32:263. [PubMed: 13679654]
29. Katiyar VK, Fisseha D. World. 2011; 1:100.
30. Ghiran IC, Zeidel ML, Shevkoplyas SS, Burns JM, Tsokos GC, Kyttaris VC. Arthritis and Rheumatism. 2011; 63:503. [PubMed: 21280005]
31. Adamo A, Sharei A, Adamo L, Lee B, Mao S, Jensen KF. Analytical chemistry. 2012; 84:6438. [PubMed: 22746217]
32. Huang, S.; Bow, H.; Diez-Silva, M.; Han, J. Massachusetts Institute of Technology, Department of Electrical Engineering and Computer Science; 2011.
33. Mairbäurl, H. Frontiers in Physiology. 2013. p. 4
34. Hosseini SM, Feng JJ. Biophysical journal. 2012; 103:1. [PubMed: 22828326]
35. Wagner GM, Chiu DT, Qju JH, Heath RH, Lubin BH. Blood. 1987; 69:1777. [PubMed: 3580578] Card R, Mohandas N, Mollison P. British journal of haematology. 1983; 53:237. [PubMed: 6821653]
36. Costa M, Ghiran I, Peng CK, Nicholson-Weller A, Goldberger AL. Physical Review E. 2008; 78:020901.
37. Chandramohanadas R, Park Y, Lui L, Li A, Quinn D, Liew K, Diez-Silva M, Sung Y, Dao M, Lim CT. PloS one. 2011; 6:e20869. [PubMed: 21698115]
38. Mohandas N, Gallagher PG. Blood. 2008; 112:3939. [PubMed: 18988878]
39. Zimrin JRHAB. Vox sanguinis. 2009; 96:93. [PubMed: 19152602]
40. Li J, Wang JP, Ghiran I, Cerny A, Szalai AJ, Briles DE, Finberg RW. Infection and immunity. 2010; 78:3129. [PubMed: 20439480]
41. Chen CH, Ghiran I, Beurskens F, Weaver G, Vincent J, Nicholson-Weller A, Klickstein L. Clinical & Experimental Immunology. 2007; 148:546. [PubMed: 17493021]
42. Gliemann L, Nyberg M, Hellsten Y. Free radical research. 2013; 1Kuo L, Thengchaisri N, Hein TW. Molecular Medicine & Therapeutics. 2012; 1
43. Grau M, Pauly S, Ali J, Walpurgis K, Thevis M, Bloch W, Suhr F. PloS one. 2013; 8:e56759. [PubMed: 23424675]
44. Bonaventura J. Proc Nat Acad Sci. 2007; 104:19165. [PubMed: 18048331]
45. Chin-Yee I, Arya N, d'Almeida MS. Transfusion science. 1997; 18:447. [PubMed: 10175158] Yoshida T, AuBuchon J, Tryzelaar L, Foster K, Bitensky M. Vox sanguinis. 2007; 92:22. [PubMed: 17181587]
46. Kriebardis AG, Antonelou MH, Stamoulis KE, Economou-Petersen E, Margaritis LH, Papassideri IS. Journal of cellular and molecular medicine. 2007; 11:148. [PubMed: 17367509]
47. Samot J, Moon S, Shao L, Zhang X, Xu F, Song Y, Keles HO, Matloff L, Markel J, Demirci U. PloS one. 2011; 6:e17530. [PubMed: 21412411]
48. Parmegiani L, Cognigni GE, Filicori M. Hum Reprod. 2009; 24:2969. [PubMed: 19749194]
49. McBurnie LD, Bardo B. Pharm Technol North America. 2002; 26:9.
50. Bielanski A, Vajta G. Hum Reprod. 2009; 24:2457. [PubMed: 19561041]

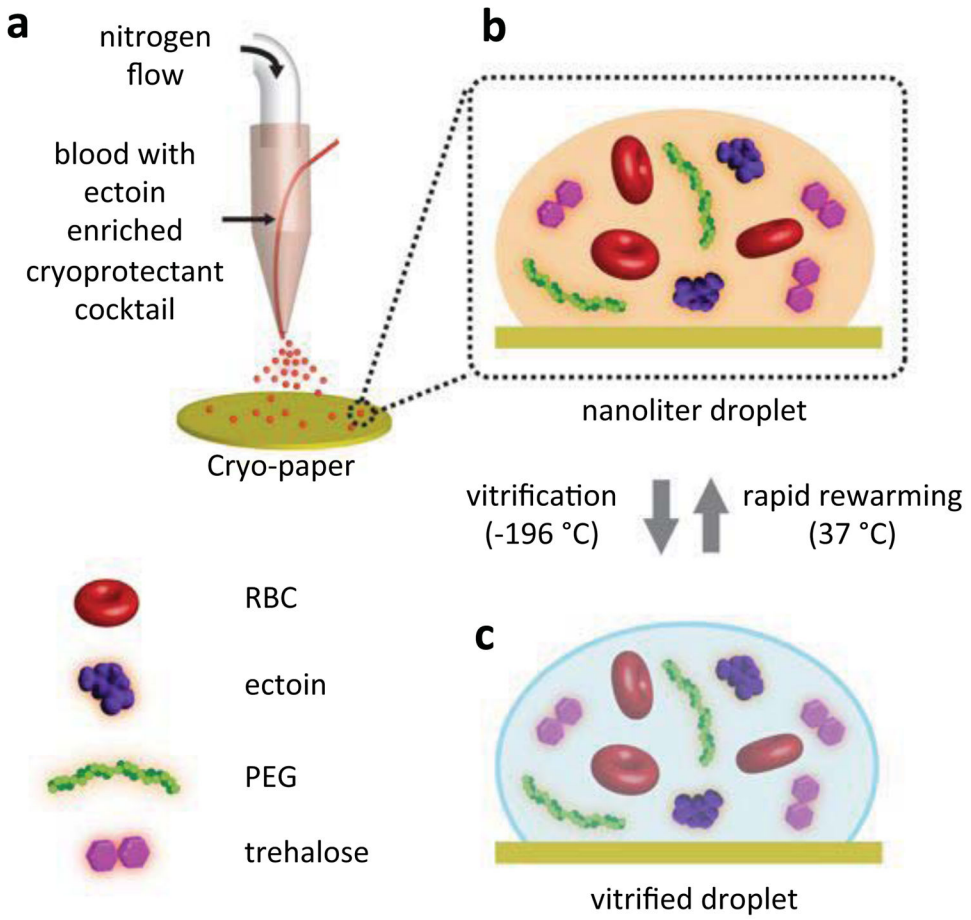

Figure 1. Droplet-based vitrification of red blood cells

a, The essentials of the experimental setup for the droplet formation. The system consists of nitrogen gas flow and a droplet deposition system controlled by a syringe pump. The droplets are generated from the co-flow stream of cryoprotective agent (CPA)-loaded red blood cell (RBC) mixture as the nitrogen gas flows through a droplet ejector, which transforms the bulk of the sample into nanoliter droplets. The CPA consists of a cocktail solution of ectoine, trehalose, and polyethylene glycol (PEG). The droplets were ejected on a cryo-paper (polyethylene collection film). **b,** The magnified view of a single droplet on the cryo-paper including RBCs, ectoine, trehalose and PEG. **c,** The view of the vitrified droplet in (b). The vitrification is achieved by submersing the cryo-paper into liquid nitrogen. The vitrified droplet transforms to (b) after rapid thawing of the cells on a cryo-paper in phosphate-buffer saline at 37 °C.

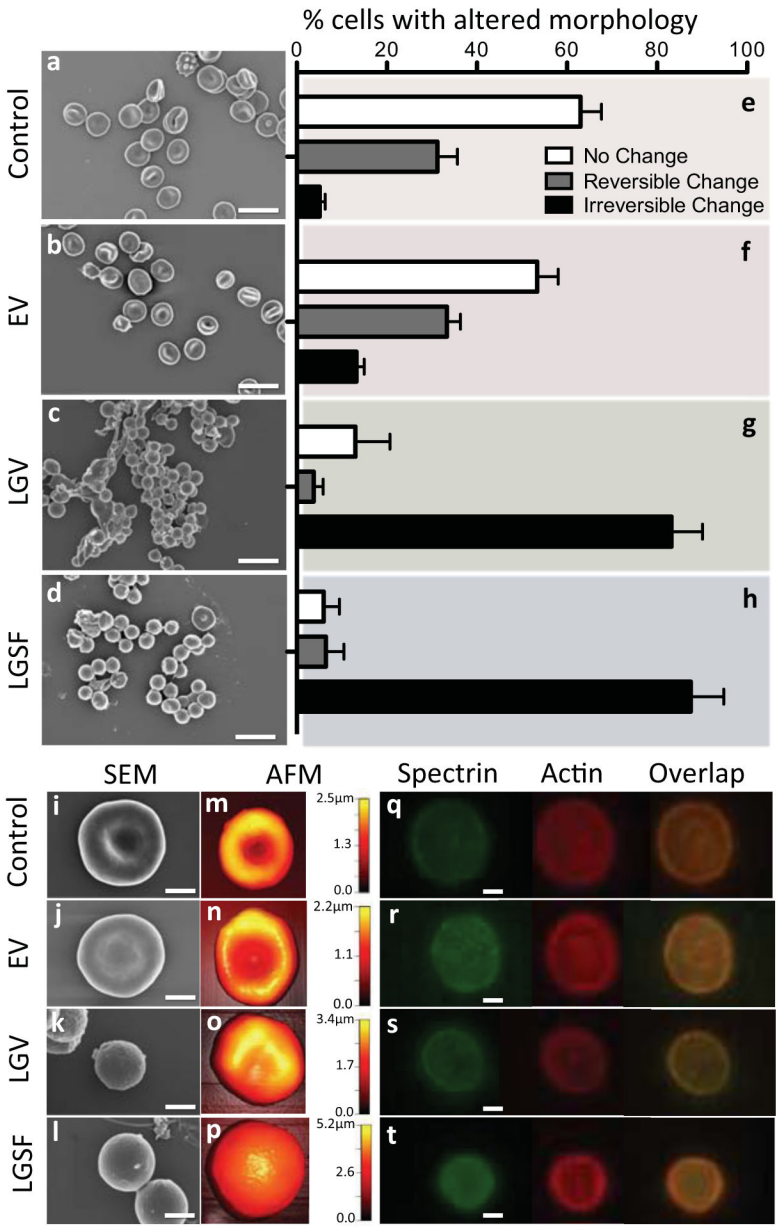

Figure 2. Assessment of RBC morphology following ectoine-based vitrification and rewarming

a–d, Scanning electron micrographs (SEMs) of RBCs (a) Selected directly from blood, recovered after (b) ectoine-based vitrification (EV), (c) low glycerol vitrification (LGV), and (d) low glycerol slow freezing (LGSF). **e–h,** The percentage (%) of RBCs within a population representing (e) untreated fresh blood, and blood recovered from (f) EV, (g) LGV and (h) LGSF: biconcave shape, and reversible and irreversible shape changes (n, number of cells =114–309 and N, number of donors =3–9). Error bars in figures represent the standard error of the mean. **i–l,** Higher magnification (30,000x) of SEMs of (i) fresh RBCs and RBCs recovered after (j) EV, (k) LGV and (l) LGSF. **m–p,** Atomic Force Micrographs (AFM) of (m) fresh RBCs and RBCs recovered after (n) EV, (o) LGV, and (p) LGSF. **q–t** Fluorescence micrographs showing distribution of the spectrin-actin network in

RBCs. (q) RBCs in fresh blood and RBCs recovered from (r) EV, (s) LGV, and (t) LGSF. Scale bar represents 10μm in **a–d** and 2μm in **i–l** and **q–t**.

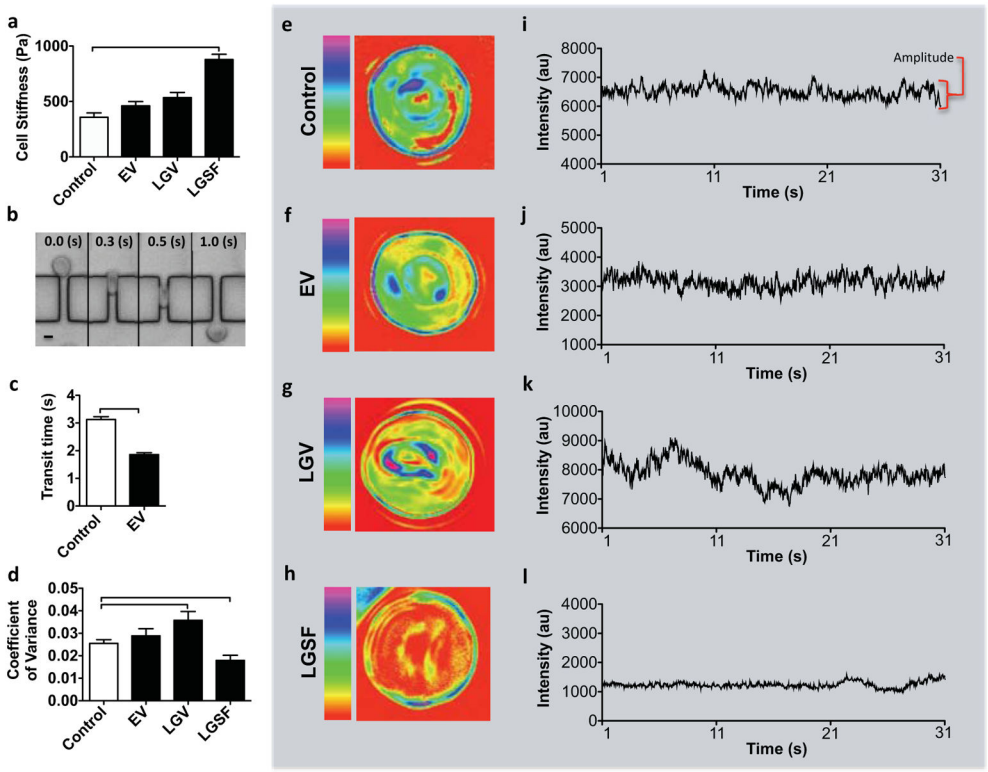

Figure 3. Assessment of RBC biomechanics following ectoine-based vitrification and rewarming

a, Cell stiffness determined via atomic force microscopy (AFM) for fresh RBCs as well as for RBCs recovered after EV, LGV, and LGSF. The measurements were performed on recovered RBCs following plasma re-suspension (n=30–45 and N=3). **b,** Light microscopy time-series of a recovered RBC (after EV) passing through the microchannel array. Scale bar represents 4μm. RBC deformability was measured as the time required for the cell to go through and exit the channel (height=2μm and width=4.5μm) **c,** Deformability determined for fresh RBCs (n=192) and for RBCs recovered after EV (n=245), N=3. **d–l** Cell membrane flickering. **d,** Membrane flickering as a function of coefficient of variance determined for fresh RBCs and RBCs recovered after EV, LGV, and LGSF, (n=14–40, N=1–3). **e–h,** Detailed flickering profiles of individual RBCs. Pseudo-color images represent a heat map of the coefficient of variance (e) of fresh RBC and recovered RBCs after (f) EV, (g) LGV, and (h) LGSF. The red-color represents minimum intensity coefficient of variance (flickering) while the magenta-color represents maximum coefficient of variance. **i–l,** Time series of coefficient of variance of a single representative pixel from heat maps of (i) fresh RBCs and recovered RBCs after (j) EV, (k) LGV and (l) LGSF. The intensity is represented in arbitrary units (au). Error bars in the figures represent the standard error of the mean. Connecting brackets between the individual groups indicate statistically significant results ($P < 0.05$).

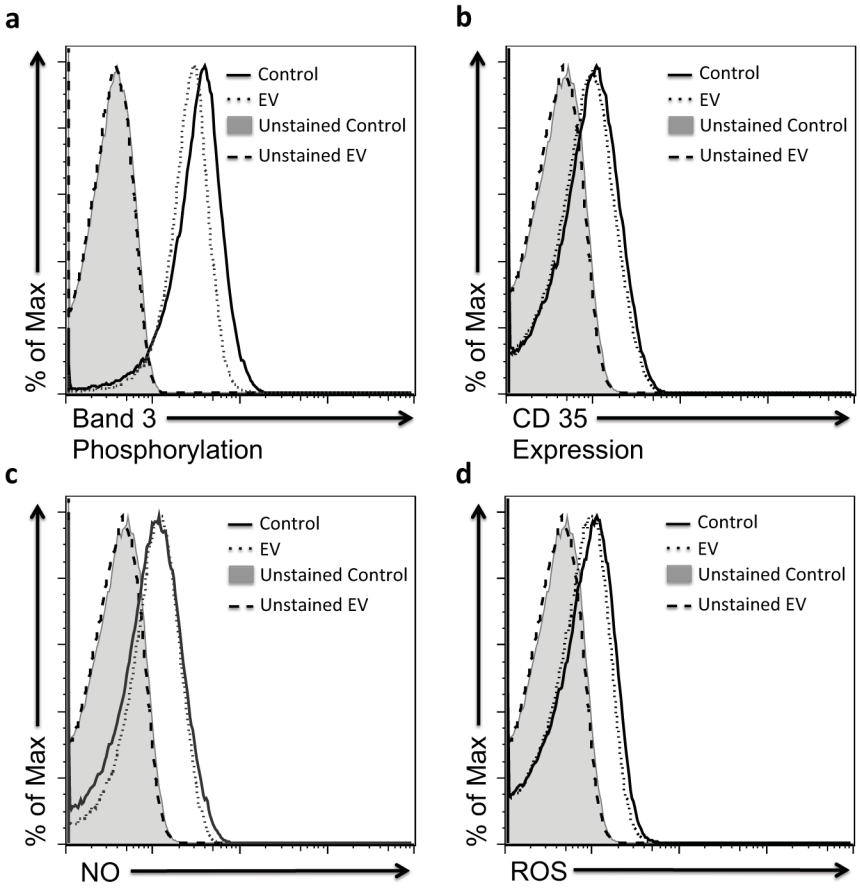

Figure 4. Assessment of RBC functional properties following ectoine-based vitrification and rewarming

a–d Functional properties for fresh RBCs (Control, solid line) and recovered RBCs after ectoine-based vitrification (EV, dotted line) were compared. Four types of characteristic RBC function were measured: (a) determined band-3 phosphorylation level, (b) CD35 expression, (c) intracellular nitric oxide (NO) level, and (d) intracellular reactive oxygen species (ROS) level. The negative controls (unstained fresh RBCs represented by the gray shaded region and unstained recovered RBCs after EV represented by the dashed line) were not labeled and used as a baseline to detect the auto-fluorescence of cells. The measurements were performed following incubation of RBCs with 25% serum from a universal acceptor for 30 mins at 37 C°.